

# Assessing the Potential of Neural Radiance Fields and Gaussian Splatting for Change Detection and Change Quantification

Lukas WINIWARTER<sup>1,\*</sup>, Frederik SCHULTE<sup>1</sup>, Jiapan WANG<sup>2</sup>, Qilin ZHANG<sup>3</sup>,  
Katharina ANDERS<sup>2</sup>, and Boris JUTZI<sup>3</sup>

<sup>1</sup> *Unit of Geometry and Surveying, Faculty of Engineering Sciences, University of Innsbruck, Innsbruck, Austria  
(lukas.winiwarter, frederik.schulte)@uibk.ac.at*

<sup>2</sup> *Remote Sensing Applications, TUM School of Engineering and Design, Technical University of Munich (TUM),  
Munich, Germany, (jiapan.wang, k.anders)@tum.de*

<sup>3</sup> *Photogrammetry and Remote Sensing, TUM School of Engineering and Design, Technical University of Munich  
(TUM), Munich, Germany, (qilin.zhang, boris.jutzi)@tum.de*

*\*corresponding author*

## Abstract

Neural Radiance Fields (NeRFs) and 3D Gaussian Splatting (3DGS) are methods alternative to multi-view-stereo (MVS) reconstruction in processing photogrammetric data. While they have been developed and optimized for creating synthetic 2D views, they are increasingly used for 3D reconstruction in the form of 3D point clouds. However, applications in geosciences are rare, and especially their suitability for change detection and quantification methods has not been assessed. In this contribution, we therefore create point clouds using state-of-the-art MVS on the one hand and NeRFs/3DGS on the other hand and compare the changes extracted from bitemporal differencing of these point clouds. For this differencing, we utilize the Multiscale Model-to-Model Cloud Comparison (M3C2) algorithm. We investigate two different study sites and include a riparian forest area as differences between MVS and NeRF/3DGS are especially pronounced in vegetated areas. For one of the areas, reference values for change are available through accurate laser scanning data. We compare the detected changes qualitatively as well as quantitatively by means of accuracy, precision, and recall. Finally, we provide conclusions for change detection and quantification with photogrammetric data using NeRFs and 3DGS.

**Keywords:** NeRF, Photogrammetry, Machine Learning, Uncertainty, Change Detection

*Received: 10<sup>th</sup> December 2024. Revised: 21<sup>st</sup> February 2025. Accepted: 7<sup>th</sup> March 2025.*

## 1 Introduction

Topographic monitoring is relevant in a wide range of applications in Earth system sciences and enables observation of surface dynamics at detailed spatiotemporal scales. Especially UAV photogrammetry has experienced a tremendous boost in applications of 3D topographic observations in the past decade, with new capabilities provided in terms of accuracy (cm-scale; compared to aerial and satellite images) and coverage (several ha; compared to ground-based strategies) (Eltner et al., 2022).

Typically, 3D models of a scene are obtained via photogrammetric reconstruction in a two-step

approach: First, images are oriented in a bundle block adjustment and are georeferenced using control points or direct georeferencing; then a pixel-by-pixel estimation of depth is carried out for each overlapping image pair to generate a dense point cloud (dense image matching DIM, multi-view-stereo MVS). With such data, change analysis is performed through multiple acquisitions that are repeated at different points in time, depending on the phenomena to be observed. Common strategies of change detection and quantification are differencing of Digital Elevation Models (DEMs), or, to maintain the full 3D character of the scene, direct point cloud comparison (Qin et al., 2016). For 3D analysis of surface changes, the state-of-the-art

is the Multi-scale Model-to-Model Cloud Comparison (M3C2) algorithm (Lague et al., 2013), which assumes local planarity of surfaces in the scene based on a user-defined set of radii that account for roughness and variable point density. From this, local distances between point positions in the scene are derived along the 3D orientation of the adjusted plane fit, and an additional estimate of the associated uncertainty is derived based on the co-registration error, local point density and surface roughness.

In recent years, alternative methods to reconstruct the 3D geometry of the scene have been presented, replacing the dense reconstruction in MVS. These methods are Neural Radiance Fields (NeRFs) and 3D Gaussian Splatting (3DGS). Both treat the reconstruction process as an optimization problem and recover the scene as a radiance field. With NeRFs, this radiance field is estimated as a neural network that maps image ray locations and directions to resulting tuples of red, green, and blue intensities, representing color. While the original idea of NeRFs was to synthesize views of the 3D scene from unobserved locations, this constitutes a 3D representation of the objects in the scene, which has already been exploited also in remote sensing applications (e.g., Ge et al., 2023). In contrast, the idea of 3DGS is the representation of the scene through 3D Gaussians, i.e., density functions typically represented by an ellipsoid. The projections of these ellipsoids on the image plane, referred to as splats, then create the colour value at a specific pixel location. When creating a 3DGS, optimization is carried out such that elongated Gaussians are split into separate components, and (almost) congruent Gaussians are merged. After optimization, the Gaussians can be exported as points with 3D direction, 3D magnitude and colour information. In contrast to a photogrammetric reconstruction, the 3D magnitudes inherently contain neighbourhood information, e.g., whether a Gaussian represents a linear or a planar feature. Missing parts in the scene, e.g. due to occlusion, are filled by the mapping to the radiance field, so that a full coverage of images of the scene is not necessary. Thereby also details in complex scenes, such as vegetation, can be better represented requiring less input data.

In this contribution, we explore the potential of point clouds directly exported from NeRF and 3DGS reconstructions for change analysis of natural scenes that are captured by UAV photography. By reconstructing two scenes at two points in time, each using the strategies of MVS, NeRF, and 3DGS,

we derive different point cloud products as input to change analysis. We quantitatively evaluate the derived changes compared to UAV-based laser scanning data for one of the datasets. Qualitative assessment of results indicate the further potential of NeRF/3DGS-based change analysis and topographic monitoring. By this, our study contributes the first insights into the direct usability of current computer vision strategies for environmental monitoring.

## 1.1 Data

Two sites of Alpine river beds and their surroundings, featuring hillslopes and vegetation, are used for the experiments, with two epochs each. One showcases a high alpine setting in Jamtal, Tyrol (WGS84: 46.8954°N, 10.1726°E) at an approximate elevation of 2000 m.a.s.l. The Jamtal river runs through the study site with maximum discharge rates  $> 15 \text{ m}^3/\text{s}$  (max. Q/day) at the investigated location (Stang, 2023). This discharge, in combination with flat terrain characterized by loose gravel in a stranded riverbed, leads to a changing topography. The investigated area measures approx. 350 x 700 m and was recorded using a calibrated DJI Zenmuse P1 camera mounted on a DJI M350 RTK quadcopter on 2024-08-27 and 2024-11-11. Both times, a laser scanning survey using a DJI Zenmuse L2 mounted on the same quadcopter, was conducted additionally, and serves as our reference dataset (see Section 2.6).

The second dataset was acquired in southern Germany, at a natural stretch of the Isar river (WGS84: 47.5301°N, 11.3090°E). The elevation of this study site is about 900 m.a.s.l. Upstream of the study site, a weir redirects water into the Obernachkanal channel, controlling discharges at the study site to limited amounts. The investigated area measures 800 x 400 m and showcases a meander of the river with an extensive gravel bed, which is limited by the steep flank into the Karwendel mountains in the North and alluvial forest on the river terrace to the South. Data was captured on 2024-08-12 and 2024-11-05 using a DJI Phantom 4 RTK UAV with built-in camera.

## 2 Methodology

We investigate the potential of NeRFs and 3DGS for topographic change detection and quantification in natural scenes. The same UAV images are used as input for all 3D reconstruction techniques, which are based on Structure-from-Motion (SfM) processing (Section 2.1) and explained in detail in

the following subsections: MVS in Section 2.2, NeRFs in Section 2.3, and 3DGS in Section 2.4. Based on point clouds derived from these strategies, we perform change detection and quantification using direct point cloud comparison (Section 2.5). The evaluation of results is based on laser scanning data as reference, as described in Section 2.6. An overview of the workflow is given in Figure 1.

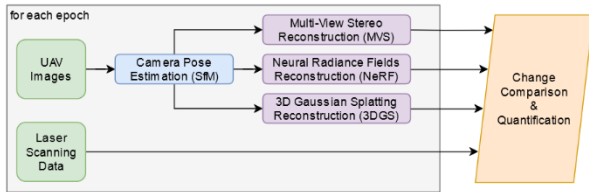


Figure 1. Diagram of the workflow carried out at each of the study sites. For the Isar study site, no laser scanner reference was used.

Results are presented in Section 3 and provide insight into the potential and limitations of each strategy, as well as directions for future research on NeRF/3DGS-based environmental monitoring.

## 2.1 SfM

Structure from Motion (SfM) is a photogrammetric technique that reconstructs 3D scenes from 2D images by simultaneously estimating camera poses and sparse 3D structure (Jäger, 2024). The process involves detecting distinctive features, such as those identified by the Scale-Invariant Feature Transform (SIFT) algorithm (Lowe, 2004) and matching them across overlapping images. Outlier rejection methods like Random Sample Consensus (RANSAC) (Fischler & Bolles, 1981) ensure reliable correspondences. Using these correspondences, initial camera poses are estimated through geometric models, enabling the triangulation of sparse 3D points. Bundle adjustment then refines the reconstruction by minimizing reprojection error and improves both camera parameters and 3D point accuracy (Triggs et al., 2000). This step ensures the geometric consistency and alignment of the sparse point cloud with the input images (Petrovska, 2024).

In our experimental framework, SfM provides the fundamental geometric foundation for subsequent reconstruction methods, including MVS, NeRFs, and 3DGS. The derived camera poses and sparse point cloud serve as initialization data and establish a common geometric reference frame.

## 2.2 MVS

The classical Multi-View Stereo (MVS) framework (Schönberger et al., 2016) is initialized by the output

of the SfM. In general, the MVS relies on principles for correspondence search but has a high complexity due to redundancy resulting from the multiple observations and the arbitrary viewpoint variations (Hermann et al., 2024). By considering multiple images of the same scene, the MVS algorithms generate a complete and dense 3D representation of the scene as a point cloud. MVS achieves high 3D reconstruction accuracy when surfaces are well textured and diffuse.

## 2.3 NeRFs

Neural Radiance Fields (NeRFs) have emerged as a technique for representing 3D scenes captured by photographs. The principle of NeRFs utilizes a neural network to predict a tuple of color (red, green, blue) and density ( $\rho$ ) for a given location in space ( $X, Y, Z$ ) and viewing direction ( $\phi, \theta$ ). A single pixel is then reconstructed by sampling and evaluating the neural network along the image ray and calculating the color value according to (a) the density at a given location and (b) the density at all locations that are between the target location and the respective camera. The density can also be interpreted as “the differential probability of a ray terminating at an infinitesimal particle at location  $x$ ” (Mildenhall et al., 2020).

Using cameras with multiple millions of pixels, training data sets of substantial size are easily created. In the optimization, the resulting colour for training pixels is calculated and compared against the observed colour. The difference is backpropagated through differentiable rendering to adapt the weights of the neural network representing the scene. While the original goal of NeRFs was view synthesis, i.e., the reconstruction of camera views from unobserved locations and orientations, we exploit the latent representation of the scene geometry through the neural network. We export a point cloud from the NeRF by sampling locations with a high density value, corresponding to a large contribution in the pixel color. This is related to the presence of an opaque object at a given location. The points are subject to a statistical outlier removal before export, ensuring that the point cloud mostly represents the actual scene geometry.

## 2.4 3DGS

3D Gaussian Splatting (3DGS) represents a novel approach to scene reconstruction that models 3D scenes as a collection of oriented 3D Gaussians (Kerbl, 2023). The approach initializes Gaussian primitives from the sparse point cloud generated by the SfM pipeline, where each Gaussian inherits its

spatial position from the corresponding 3D point and adopts the associated color as its initial appearance attribute. Each Gaussian is defined by its mean position  $\mu \in \mathbb{R}^3$ , a rotation matrix  $R \in \mathbb{R}^{3 \times 3}$ , and scaling factors  $s \in \mathbb{R}^3$ , which together define its covariance matrix  $\Sigma$ . Additionally, an opacity value  $\alpha$  controls transparency, while spherical harmonics coefficients are used to model view-dependent appearance effects. During optimization, the parameters of the Gaussians are refined through a differentiable rasterization pipeline. This process begins by sorting the Gaussians along each camera ray based on their mean positions, ensuring a correct ordering for subsequent rendering. Each 3D Gaussian is then projected onto the image plane as a 2D Gaussian splat, with its anisotropic properties preserved under perspective projection. Contributions from overlapping Gaussians are accumulated using  $\alpha$ -compositing, where the opacity value  $\alpha$  determines the influence of each Gaussian on the final rendered pixel. The rendered images are compared against ground truth images using a photometric loss function, which drives the refinement of all Gaussian parameters, including their positions, scales, rotations, opacities, and color attributes. To further improve efficiency and quality, the optimization process dynamically adjusts the number and distribution of Gaussians by performing density-based pruning and splitting operations, which ensures a compact yet accurate representation of the scene.

A key advantage of 3DGS lies in its ability to achieve high-quality real-time rendering. However, its geometric accuracy in 3D reconstruction requires further investigation (Zhang, 2024). To create point clouds from 3DGS scenes, we extract the centroids of the generated Gaussians and compare the results with those obtained from traditional MVS methods and NeRF. This comparative evaluation allows us to assess 3DGS's performance in geometric reconstruction and explore its potential for change detection applications.

## 2.5 Change Detection and Quantification

The primary interest of our applications is to derive surface changes that typically represent sediment transport in our study sites (e.g. transport of bed load through water discharge). This is manifested in increase or decrease of elevation in the riverbed, which can be extracted by direct point cloud comparison of the surface representation in a straight-forward way.

Change detection and quantification of bitemporal point clouds for each of the strategies (MVS, NeRF, 3DGS) is therefore performed using the state-of-the-art M3C2 algorithm (Lague et al., 2013). We use a multi-scale normal radius of 0.25 m to 1.0 m (0.25 m steps, maximizing planarity) for the plane adjustment to the local surface, which determines the direction of change estimation. The projection radius defines the neighborhood of 3D points that are used to estimate the local surface. We set this radius to 0.5 m. The same parameters are used for both sites as they feature similar surface characteristics and, accordingly, roughness scales. To estimate the minimum detectable change (*Level of Detection*), we apply a significance threshold of 95%.

We do not consider (changes of) vegetation in the scene in the frame of this study, as this will require a different approach of change detection. However, as vegetation is only featured in the Isar study site, we also have no suitable laser scanning reference data for evaluation of this part of the scene and potentially observed changes (cf. Section 2.6).

## 2.6 Evaluation

For the Jamtal dataset, the changes derived for each 3D reconstruction strategy are evaluated against a UAV laser scanning point clouds. Regarding the measuring principles, we can assume that the LiDAR acquisitions in general provide more accurate representations of the scene and consequently of changes between the epochs. We can, therefore, conduct an appropriate relative assessment of change detection and quantification. A quantitative assessment of absolute changes is not possible, since there is no ground-truth data available for either study site. However, visual interpretation of change information will provide some insight into the process types and scales that can be observed.

## 3 Results & Discussion

In the following, the point clouds obtained using the three investigated photogrammetric methods are presented (Sections 3.1-3.3) along with the result of the change detection and quantification (Sect. 3.4).

### 3.1 MVS

MVS was performed using Agisoft Metashape (v2.1.3) for the Jamtal dataset (Fig. 2) and Pix4Dmatic (v1.68.1) for the Isar river dataset (Fig. 3).



Figure 2. MVS results of the Jamtal River site from bi-temporal datasets (left: Aug., right: Nov. 2024).

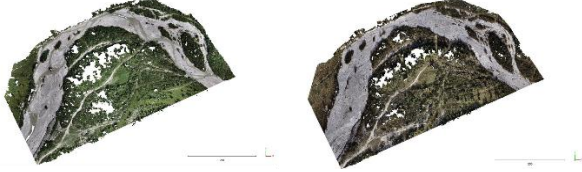


Figure 3. MVS results of the Isar River site from bi-temporal datasets (left: Aug., right: Nov. 2024).

### 3.2 NeRF

For the NeRF reconstruction, we used the Nerfacto model implemented in Nerfstudio (Tancik et al., 2023). The resulting point clouds for the Jamtal dataset are shown in Fig. 4. In the detail view, typical artefacts of NeRFs, i.e., large undulations in the terrain, can be clearly seen. Fig. 5 shows the rendered NeRF point cloud for the Isar dataset. In the oblique views, the successful reconstruction of the tree crowns in the riparian forest can be seen. The riverbed exhibits undulations similar, albeit less pronounced than with the Jamtal dataset (Fig. 4). Initial experiments with less accurate projection center locations (lower-quality SfM reconstruction) showed large systematic deviations, highlighting the need for a solid bundle block adjustment prior to NeRF reconstruction. As shown in Table 1, the number of points exported from the NeRF is similar to the MVS points for the Jamtal dataset, but significantly lower for the Isar dataset to keep noise at a plausible level.

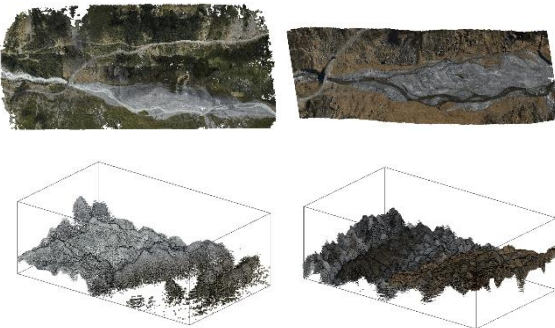


Figure 4. NeRF results of the Jamtal River site from bi-temporal datasets (left: August, right: November 2024). Top: top-down view on the full dataset, bottom: detail view on the riverbed, box size approx. 15x30 m).



Figure 5. NeRF results of the Isar River site from bi-temporal datasets (left: Aug., right: Nov. 2024). Top: top-down view, bottom: oblique view).

### 3.3 3DGS

For the 3DGS reconstruction, we used the Gaussian Splatting PyTorch Lightning Implementation (<https://github.com/yzslab/gaussian-splatting-lightning>). This implementation allows us to train on high-resolution original images while avoiding memory overflow. The reconstruction results are presented in Figures 6 and 7. In contrast to the MVS and NeRFs visualisations, we additionally show the render result, i.e., the reconstruction as used for the 3DGS optimization. The top row (a,b) shows this rendered reconstruction. Below these, (c,d) display the centroids of the extracted Gaussians represented as point clouds of the complete scene, coloured by distance to the viewing plane. The detailed views (e,g) demonstrate the rendering quality of selected regions, while (f,h) show their corresponding point cloud representations.

Table 1. Number of points (in millions [M]) for each of the reconstruction methods, epochs, and datasets. For 3DGS, the number of 3D Gaussians is given.

| Dataset/<br>Epoch | Points<br>ULS | Points<br>MVS | Points<br>NeRF | 3DGS |
|-------------------|---------------|---------------|----------------|------|
| Jamt. 08-27       | 182M          | 393M          | 299M           | 8M   |
| Jamt. 11-11       | 53M           | 477M          | 480M           | 8M   |
| Isar 08-12        | N/A           | 58M           | 5M             | 3M   |
| Isar 11-05        | N/A           | 314M          | 4M             | 3M   |

### 3.4 Change Detection and Quantification

From the extracted point clouds, bitemporal change values were derived using the M3C2 algorithm. The results of the M3C2 algorithm, including the derived change, the associated uncertainty, and binary change maps, are shown in Figures 8 and 9. The change was evaluated at core point locations, a subsampled point cloud with approx. 20M points for

Jamtal and 46M points for the Isar dataset, respectively.

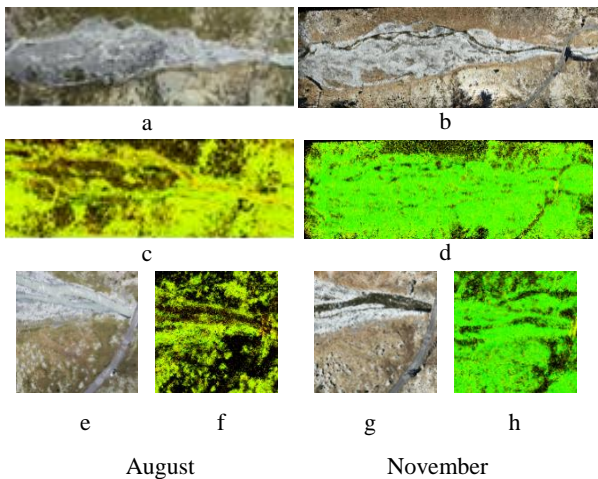


Figure 6. 3DGS results of the Jamtal River site (August and November 2024). (a,b) Full scene renderings; (c,d) Extracted point clouds of the complete scene; (e,g) Zoomed-in renderings showing detail preservation; (f,h) Detailed point cloud views of the selected region.

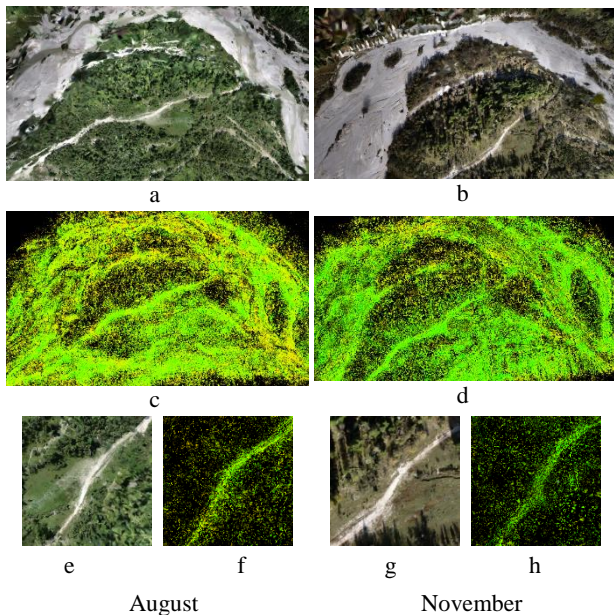


Figure 7. 3DGS results of the Isar River site (August and November 2024). Layout of renderings and point clouds follows the same arrangement as Figure 6.

For quantitative evaluation of the change result, we use the binary UAV laser scanning (ULS) change map as reference to compare with the three photogrammetric datasets, calculating the accuracy, precision, and recall values (Table 2), where accuracy is the percentage of points correctly identified as change or no change, precision is the number of points correctly identified as change (true positives, TP) in relation to the number of TP and FP, and recall is the number of true positives in relation to TP and FN.

Table 2. Performance of the change detection using different reconstruction methods for the Jamtal.

| Score         | MVS   | NeRF  | 3DGS  |
|---------------|-------|-------|-------|
| Precision [%] | 93.98 | 88.33 | 48.09 |
| Recall [%]    | 43.10 | 10.83 | 12.05 |
| Accuracy [%]  | 86.76 | 20.43 | 55.10 |

As seen in Figs. 8 and 9 and Table 2, applying change detection directly on the exported NeRFs and 3DGS performs – in general – more poorly than standard MVS. While 3DGS tends to perform better than NeRFs (Tab. 2), the spatial coverage is much more inhomogeneous than with NeRFs (Figs. 8 and 9). In the riparian woodland area of the Isar study site, false positives can be seen in the MVS result, that are not present in the NeRF or 3DGS results, pointing to a misrepresentation of vegetation in the MVS due to the inherent smoothness constraint in the reconstruction. Both NeRFs and 3DGS are radiance field methods optimizing the object space representation such that it best recreates the camera views. Especially for 3DGS, this means that the centroids do not represent a surface, as is the case with laser scanning and MVS. With NeRFs, the large terrain undulations for the Jamtal dataset can be explained by the lack of oblique imagery. The Isar dataset shows less of these effects, (cf. significant change quantification in Fig. 9, right column). Notably, the riverbed (where change is expected) and some of the paths through the riparian woodlands (where no change is expected) are flagged as significant change, while the forested area is correctly not marked as significant change.

## 4 Conclusion

While Neural Radiance Fields (NeRFs) and 3D Gaussian Splatting (3DGS) show promising results in 3D scene representation, especially with complex objects such as vegetation, a direct application of change detection and quantification methods established for point clouds did not show promising results. On flat and planar objects, the smoothness constraint of Multi-View-Stereo reconstructions complements the planarity constraint of the M3C2 algorithm. This shows that further research is required to better transfer existing methods for topographic change quantification and detection. Especially the quantification of local uncertainty, for which M3C2 relies on estimating the quality of a planar fit, should be revisited as it could be evaluated via the density gradient for NeRFs and via the axis definitions of the individual Gaussians for 3DGS.

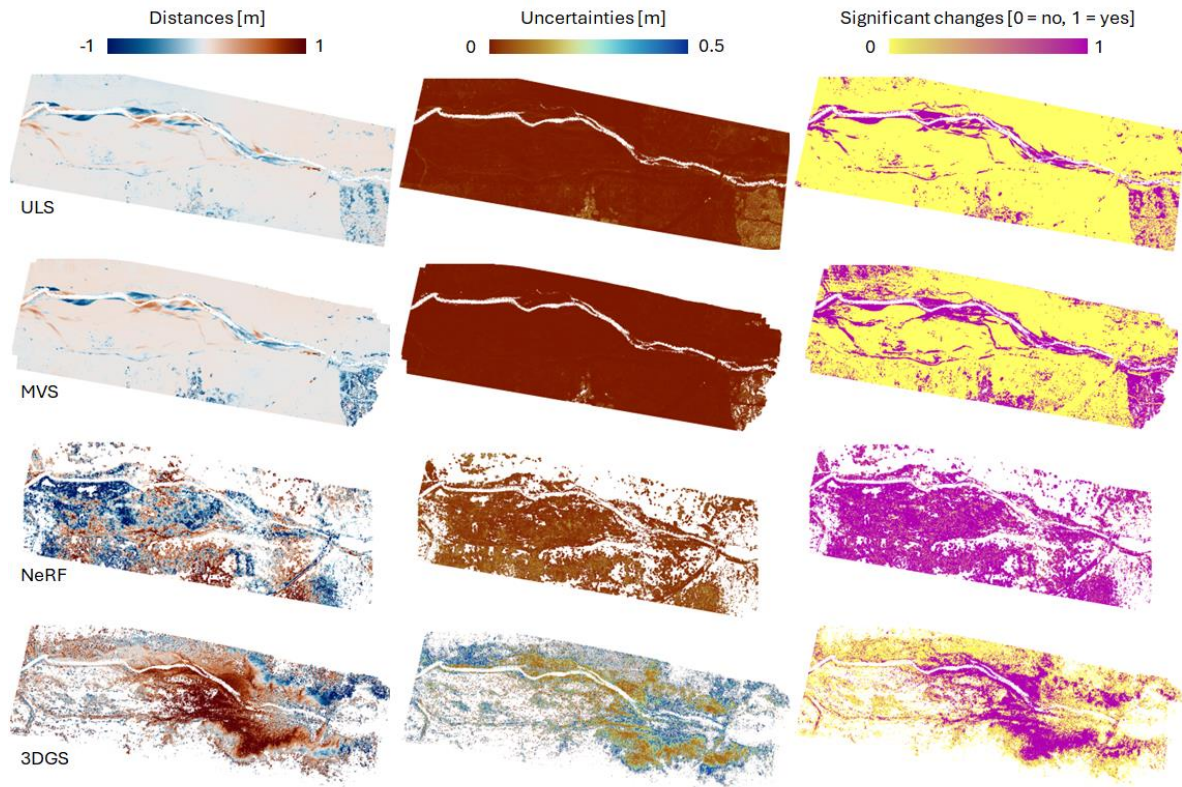


Figure 8. Change detection and quantification results of the Jamtal River site from bi-temporal datasets (August and November 2024) for each dataset: UAV laser scanning (reference), MVS, NeRF, 3DGS.

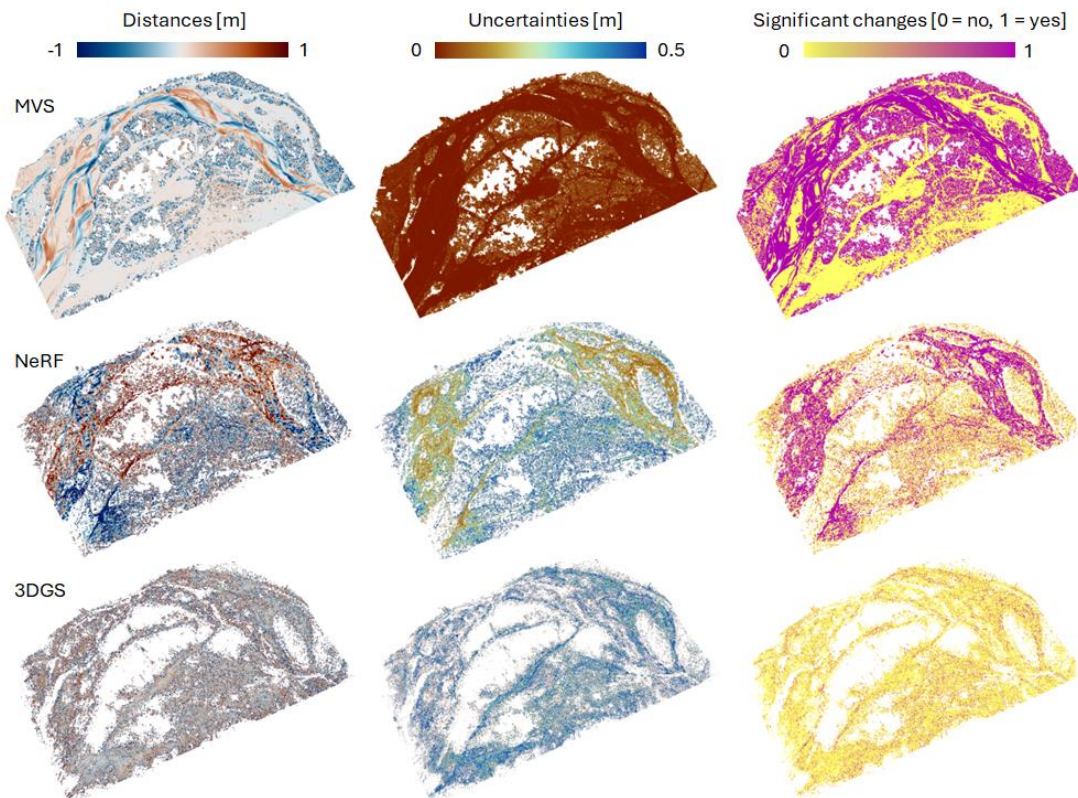


Figure 9. Change detection and quantification results of the Isar River site from bi-temporal datasets (August and November 2024) for each dataset: MVS, NeRF, 3DGS.

## References

- Eltner, A., Hoffmeister, D., Kaiser, A., Karrasch, P., Klingbeil, L., Stöcker, C., & Rovere, A. (2022): UAVs for the Environmental Sciences – Methods and Applications. Retrievable from [https://www.herder.de/-/media/files/herder/zusatzdownloads/9783534405909\\_OA.pdf](https://www.herder.de/-/media/files/herder/zusatzdownloads/9783534405909_OA.pdf) (2024-12-04).
- Fischler, M. A., & Bolles, R. C. (1981). Random sample consensus: a paradigm for model fitting with applications to image analysis and automated cartography. *Communications of the ACM*, 24(6), 381-395.
- Ge, H., Zhu, Z., Qiu, H., & Zhang, Y. (2023). Neural Radiation Fields in a Tidal Flat Environment. *Applied Sciences*, 13(19), 10848. doi: 10.3390/app131910848.
- Hermann, M., Weinmann, M., Nex, F., Stathopoulou, E.K., Remondino, F., Jutzi, B., & Ruf, B. (2024) Depth estimation and 3D reconstruction from UAV-borne imagery: Evaluation on the UseGeo dataset. *ISPRS Open Journal of Photogrammetry and Remote Sensing* doi: 10.1016/j.ophoto.2024.100065.
- Jäger, M., Kapler, T., Feßenbecker, M., Birkelbach, F., Hillemann, M., & Jutzi, B., 2024. HoloGS: Instant Depth-based 3D Gaussian Splatting with Microsoft HoloLens 2. *The International Archives of the Photogrammetry, Remote Sensing and Spatial Information Sciences*, XLVIII-2-2024, 159-166. doi:10.5194/isprs-archives-XLVIII-2-2024-159-2024
- Kerbl, B., Kopanas, G., Leimkühler, T., & Drettakis, G. (2023). 3D Gaussian Splatting for Real-Time Radiance Field Rendering. *ACM Trans. Graph.*, 42(4), 139-1.
- Mildenhall, B., Srinivasan, P. P., Tancik, M., Barron, J. T., Ramamoorthi, R., & Ng, R. (2020). NeRF: Representing scenes as neural radiance fields for view synthesis. In *Proceedings of the European Conference on Computer Vision (ECCV)*.
- Lague, D., Brodu, N., & Leroux, J. (2013). Accurate 3D comparison of complex topography with terrestrial laser scanner: Application to the Rangitikei canyon (N-Z). *ISPRS Journal of Photogrammetry and Remote Sensing*, 82. doi: 10.1016/j.isprsjprs.2013.04.009.
- Lowe, D. G. (2004). Distinctive image features from scale-invariant keypoints. *International Journal of Computer Vision*, 60, 91-110.
- Petrovska, I., & Jutzi, B., 2024. Vision through Obstacles: 3D Geometric Reconstruction and Evaluation of Neural Radiance Fields (NeRFs). *Remote Sensing*, 16(7), 1188.
- Qin, R., Tian, J., & Reinartz, P. (2016). 3D change detection Approaches and applications. *ISPRS Journal of Photogrammetry and Remote Sensing*, 122. doi: 10.1016/j.isprsjprs.2016.09.013.
- Schönberger J. L., Zheng E., Frahm J.-M., & Pollefeys M. (2016) Pixelwise View Selection for Unstructured Multi-View Stereo. *European Conference on Computer Vision*, Springer, 501–518.
- Stang, A. K. (2023). Analyzing peak flow response to meteorological conditions and hydrological modeling in Jamtal valley (*Master's thesis*). University of Innsbruck, Department of Geo- and Atmospheric Sciences, Institute of Geography.
- Tancik, M., Weber, E., Ng, E., Li, R., Yi, B., Kerr, J., Wang, T., Kristoffersen, A., Austin, J., Salahi, K., Ahuja, A., McAllister, D., & Kanazawa, A. (2023). Nerfstudio: A modular framework for neural radiance field development. In *ACM SIGGRAPH 2023 Conference Proceedings (SIGGRAPH '23)*.
- Triggs, B., McLauchlan, P. F., Hartley, R. I., & Fitzgibbon, A. W. (2000). Bundle adjustment—a modern synthesis. In *Vision Algorithms: Theory and Practice: International Workshop on Vision Algorithms* Corfu, Greece, September 21–22, 1999 Proceedings (pp. 298-372). Springer Berlin Heidelberg.
- Zhang, Q., Wysocki O., Urban, S., & Jutzi, B. (2024) CDGS: Confidence-Aware Depth Regularization for 3D Gaussian Splatting. *The International Archives of the Photogrammetry, Remote Sensing and Spatial Information Sciences XLVIII-2-W7-2024-189-2024*, 189-196. doi: 10.5194/isprs-archives-XLVIII-2-W7-2024-189-2024